Lab on a Chip

PAPER

View Article Online
View Journal | View Issue

Cite this: *Lab Chip*, 2014, **14**, 2428

Dissolution without disappearing: multicomponent gas exchange for CO_2 bubbles in a microfluidic channel†

Suin Shim,[a] Jiandi Wan,[b] Sascha Hilgenfeldt,[c] Prathamesh D. Panchal[b] and Howard A. Stone*[a]

Received 21st March 2014,
Accepted 16th May 2014

DOI: 10.1039/c4lc00354c

www.rsc.org/loc

We studied the dissolution dynamics of CO_2 gas bubbles in a microfluidic channel, both experimentally and theoretically. In the experiments, spherical CO_2 bubbles in a flow of a solution of sodium dodecyl sulfate (SDS) first shrink rapidly before attaining an equilibrium size. In the rapid dissolution regime, the time to obtain a new equilibrium is 30 ms regardless of SDS concentration, and the equilibrium radius achieved varies with the SDS concentration. To explain the lack of complete dissolution, we interpret the results by considering the effects of other gases (O_2, N_2) that are already dissolved in the aqueous phase, and we develop a multicomponent dissolution model that includes the effect of surface tension and the liquid pressure drop along the channel. Solutions of the model for a stationary gas bubble show good agreement with the experimental results, which lead to our conclusion that the equilibrium regime is obtained by gas exchange between the bubbles and liquid phase. Also, our observations from experiments and model calculations suggest that SDS molecules on the gas–liquid interface form a diffusion barrier, which controls the dissolution behaviour and the eventual equilibrium radius of the bubble.

Introduction

The dissolution of CO_2 in liquid plays an important role in many environmental and energy studies. Dissolution of CO_2 in a deep saline aquifer, for example, is relevant to proposed and ongoing demonstrations of CO_2 capture and storage.[1–4] In addition, chemical reduction of CO_2 to methanol and dimethyl ether, which generates liquid fuels, requires the understanding of CO_2 dissolution in aqueous or organic media.[5–7] Furthermore, micro-scale control of the dissolution of CO_2 gas bubbles to generate micro-particles is studied actively for developing materials for targeted drug delivery, among other applications.[8–10]

The most common approach to study CO_2 dissolution in liquid is the observation of the buoyancy-driven rise of CO_2 bubbles in various liquids. Experimental and theoretical studies on the dissolution of such CO_2 bubbles document the effect of pressure,[11] salinity gradient,[12,13] and different surface tensions[14] on CO_2 bubble dissolution. For theoretical studies, a dissolution model for a stationary gas bubble, which describes the dissolution dynamics in an infinite liquid phase, was proposed by Epstein and Plesset, who solved the one-dimensional (radial) diffusion equation to predict the time-dependent dynamics of a spherical bubble of a single gas component:[15,16] a bubble in an under-saturated solution was calculated to shrink, and does so at increasing rate, until it eventually disappears. Bubble growth in an over-saturated solution was predicted to show a nearly linearly increasing trend of the bubble radius with time. These studies have some resemblance to classical work in chemical engineering on gas–liquid adsorption/desorption processes (see the chapter 22 in the ref. 17).

To treat a multicomponent dissolution model Weinberg and Subramanian described the behaviour of an isolated gas bubble in a glass-melt under a multi-gas environment. The authors considered a spherical gas bubble that has more than one gaseous component, and solved a series of radial diffusion equations to obtain the radius change and variation of partial pressures of the different components in the bubble.[18] According to this multicomponent dissolution model, a bubble that is initially 100% O_2 will shrink in the beginning and reach a finite radius, whereas a bubble that is initially 100% CO_2 is predicted to grow in the early stage due to O_2 influx, and shrink after reaching the maximum radius. Also, the effects of surface tension on gas bubble dissolution and growth have been studied from which surface

[a] *Department of Mechanical and Aerospace Engineering, Princeton University, Princeton, NJ, USA. E-mail: hastone@princeton.edu*
[b] *Microsystems Engineering, Rochester Institute of Technology, Rochester, NY, USA*
[c] *Department of Mechanical Science and Engineering, University of Illinois, Urbana Champaign, IL, USA*

† Electronic supplementary information (ESI) available. See DOI: 10.1039/c4lc00354c

tension promotes dissolution and slows down the growth of bubbles.[19] These classic theoretical studies on single gas bubble dissolution show solutions of the radial diffusion equation at different conditions, but the predictions are limited to slowly dissolving bubbles since the transient part of the equation was often neglected. Also, due to lack of experimental data, tests of the model were absent in such studies.

Recent advances in microfluidics have enabled the controlled generation of microbubbles and the examination of the dynamics of microbubbles with a high spatio-temporal resolution. In particular microfluidic demonstrations of the formation of CO_2 bubbles in liquid,[20–28] have included CO_2 degassing in micro fuel cells,[7] observation of large elongated CO_2 slugs,[20,21] pH and temperature effects on CO_2 bubbles,[26,28] and generation of CO_2 armored bubble with colloidal particles.[25] To the best of our knowledge, there are no reports of the study of the dynamics of CO_2 bubble dissolution as it is affected by gas exchange in a microfluidic channel flow because of the short time scales and difficulty in controlling micrometer-sized bubbles. Understanding the dissolution of CO_2 gas bubbles in small devices can lead to technical improvements of microsystems such as designing micro fuel cells. Also, our study of CO_2 bubbles, which considers the effects of gas components other than CO_2, may impact further microfluidic studies including gas exchange.

In this study, we explore the dynamics of the dissolution of CO_2 microbubbles in sodium dodecyl sulfate (SDS) solutions and show that there are two regimes of dissolution of CO_2 bubbles during flow in a microfluidic channel. The first regime is a rapid dissolution regime, where the bubble size decreases rapidly within 30 ms. The second regime of dissolution is an apparent equilibrium, where the size of the bubbles remains constant during flow along the channel. This observation appears unexpected since the solution is not saturated with CO_2, so bubble dissolution might be expected. We rationalize our observations by considering other gas species, *e.g.* the components in air that are already dissolved in the liquid phase, and explain the results quantitatively by applying a modified multicomponent dissolution model. Comparisons between the experimental results and the model calculations are presented. Based on the results, we suggest that surfactant molecules control gas exchange during the early stage of bubble dissolution.

Experiment

Setup and materials

CO_2 microbubbles are generated in aqueous SDS solutions by using flow-focusing microfluidic channels (Fig. 1(a, b)). The initial bubble diameter and the distance between the bubbles are maintained constant by choosing flow rates and gas pressures, whereas the concentration of SDS is varied in different experiments. The channels were fabricated in polydimethylsiloxane (PDMS) using standard soft photolithography techniques. The width and height of the main channel where the liquid and bubbles flow together are, respectively, 150 μm and 38 μm.

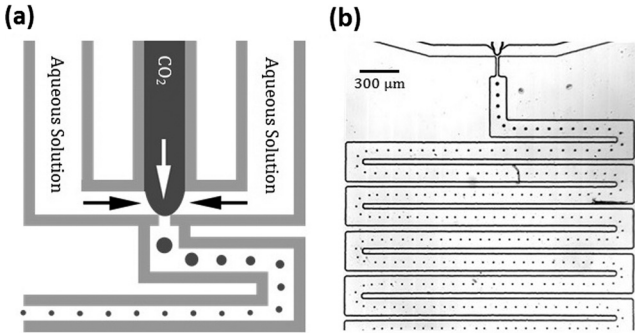

Fig. 1 (a) Schematic diagram of the experiment in a flow-focusing microfluidic device. In the liquid phase, the concentration of SDS was varied from 0.5 mM to 20 mM (CMC of SDS = 8 mM). (b) High-speed photo taken in a 10 mM experiment – scale bar is 300 μm. Water flow rate: 27 μL min^{-1}; CO_2 inlet pressure: 7 psi. The CO_2 bubbles shrink initially then reach a steady-state size.

A schematic drawing of the bubble generation at the flow-focusing inlet is shown in Fig. 1(a) and an image of bubbles in the microfluidic channel is shown in Fig. 1(b). The image makes clear the time evolution of the bubble since position along the channel corresponds to the time the bubble has been in contact with the solution. The trend in dissolution, and the apparent steady-state bubble size that is established, which are clearly shown in the figure, are the main themes of our paper.

For the surfactant solutions, SDS and deionized (DI) water were used. The solution was loaded in a syringe and pumped into the channel by a syringe pump (Harvard Apparatus). CO_2 gas was injected into the channel from a compressed gas tank, and the gas pressure was controlled by a pressure gauge (Victor Equipment Company) with a precision of 0.1 psi.

Before each experiment, the PDMS channel was plasma oxidized so that the surface would be hydrophilic, which makes water wet all of the inner surfaces so that the bubbles remain in the liquid phase. In our experiments, the initial bubble size, the distance between the bubbles, and the concentration of SDS in the aqueous phase are three important variables that could affect the dissolution rate. Among these factors, the concentration of SDS was chosen as a control variable while others were kept constant since they have been studied frequently. Typical flow speeds and gas injection pressures were, respectively, 8 cm s^{-1} and 7 psi. By controlling these parameters, we could maintain the initial bubble radius and the distance between the bubbles almost constant at, respectively, 30 μm and 150 μm. The concentrations of the SDS solutions were 0.5, 1, 4, 5, 8, 10, 15, and 20 mM while the critical micelle concentration (CMC) of SDS is 8 mM. Hence, we varied concentrations from much below to 2.5 times the CMC. At the highest concentration of SDS we used, the viscosity of the solution is very nearly the same as the viscosity of water.[29] Also, the surface tension of a clean

air–water interface is 72 mN m^{-1}, and the CO_2–water interface has a typical surface tension on the order of 10 mN m^{-1} in the presence of surfactants (see Fig. 2 in ref. 30).

We also performed experiments with degassed liquid. Degassing was done by using both a laboratory vacuum system and a sonicator (Cole-Parmer), and experiments were performed within 2–3 minutes after degassing. For these additional experiments, SDS was dissolved in the sonicated DI water (the cylinder was placed under vacuum while sonicating), and then the resulting solution was sonicated again before use.

The dissolution of CO_2 bubbles in the microfluidic channel flow was observed using a high-speed video camera (Phantom V9, 1400 frames per second) mounted on an inverted microscope (Leica DMI 4000B). Since the system was operated at steady state (Fig. 1(b)), one frame for each experiment was taken and the bubble area was analysed by an image analysis program in Matlab®. Typical bubble radii are the order of magnitude of 10 microns, which is much smaller than the channel height, so that after formation the bubbles are spherical for all times in the experiments.

Results

The influence of surfactant. For all of the concentrations of SDS we observe the same two regimes of the dissolution of CO_2 bubbles: first, there is a rapid dissolution regime, and second, an apparent equilibrium regime where the bubble size has stopped changing.

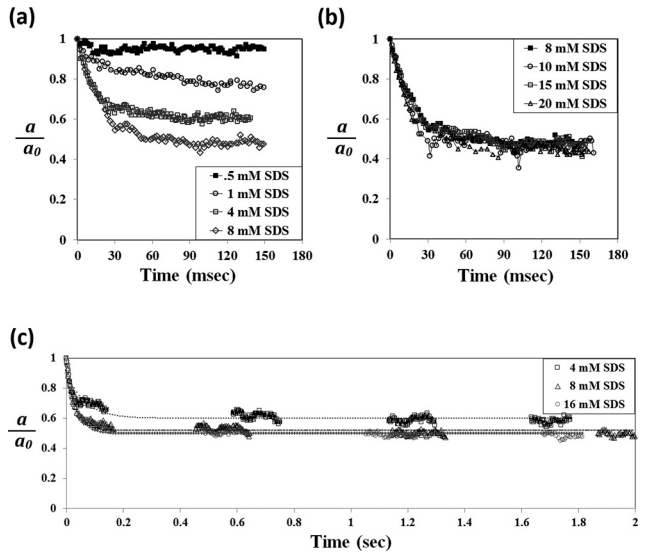

Fig. 2 Change of the nondimensional bubble radius (a/a_0) as a function of time at different concentrations of SDS. In the experiments, the bubble radii and the distance of each bubble from the flow-focusing inlet were measured. Time – the x-axis – was obtained by dividing the distance x from the entrance along the channel with the mean flow velocity $\langle v \rangle$, *i.e.* $t = x/\langle v \rangle$. (a) The bubble size, reported as a fraction of the original radius, for concentrations of SDS below the CMC. (b) The bubble size, reported as a fraction of the original radius, for concentrations of SDS above the CMC. (c) Experiments in long channels to observe dissolution over longer times. Results are shown for 4 mM, 8 mM, and 16 mM solutions, which are, respectively, 0.5 CMC, 1 CMC, and 2 CMC. Dotted lines are the fitting curves based on an exponential decay function. The typical initial radius of the bubbles was controlled to be $a_0 \approx 15$ μm for all experiments.

In Fig. 2(a–c), we summarize our results for the dissolution of CO_2 bubbles in different concentrations of SDS solutions. The bubbles shrink rapidly in approximately the first 30 ms for all concentrations of SDS (Fig. 2(a, b)), until the radius obtains a constant value. In addition, we note that the first regime of the rapid dissolution of CO_2 bubbles is affected significantly by the concentration of SDS: below the CMC (~8 mM), the bubbles dissolve faster and reach smaller equilibrium radii with an increase of the SDS concentration. In contrast, when the concentration of SDS is higher than CMC, the dissolution of CO_2 was independent of the SDS concentration (Fig. 2(b)). These results suggest that the dissolution is affected by the interaction between the surfactant and the gas bubble, and micelle formation in the liquid phase.

In a long microfluidic channel, on the other hand, we observed that CO_2 microbubbles with initial radii of 15 μm could maintain their equilibrium sizes for at least 2 seconds (Fig. 2(c)). Given that the first regime of dissolution is controlled by the surfactants, which will be discussed more in the later sections, the appearance of the equilibrium regime, however, is counterintuitive. Theoretically, as is well known[15] when a single CO_2 bubble with an initial radius of $a_0 = 15$ μm starts to dissolve in an infinite water phase, it will disappear within ~20 ms (ESI†). There is no way to achieve an equilibrium regime unless (i) the liquid phase is saturated with CO_2, which turns off the gas dissolution, (ii) there is local saturation of CO_2 near the bubble, which at least temporarily reduces the dissolution significantly and leads to the equilibrium, or (iii) other dissolved gases in the liquid diffuse into the CO_2 bubbles to compensate for the gas pressure change due to the dissolution of CO_2 which will result in an equilibrium.

Remarks about dissolution rates. We first consider the possibility of the saturation of CO_2 in the liquid phase. A few milliseconds after bubble generation, the bubble, which is much smaller than the channel dimensions, slows down and flows along with liquid. Buoyancy effects at this scale are negligible. Therefore, the bubble speed is almost the same as the liquid speed. In the bubble's reference frame, we consider that the gas is dissolving in the middle of a liquid box with dimension of $d \times w \times h$, where d is the distance between two adjacent bubbles, and w and h are, respectively, the width and height of the channel (Fig. 3(a, b)). Assuming the liquid is pure water, and using the solubility of CO_2 in water at room temperature and atmosphere pressure, the amount of CO_2 gas in the initial bubble introduced in the channel is negligibly small compared to the amount of CO_2 that can dissolve into the volume of water surrounding the bubble (ESI†). This calculation is reasonable because the liquid and CO_2 gas meet immediately before entering the orifice of the flow-focusing channel, and thus the initial concentration of CO_2

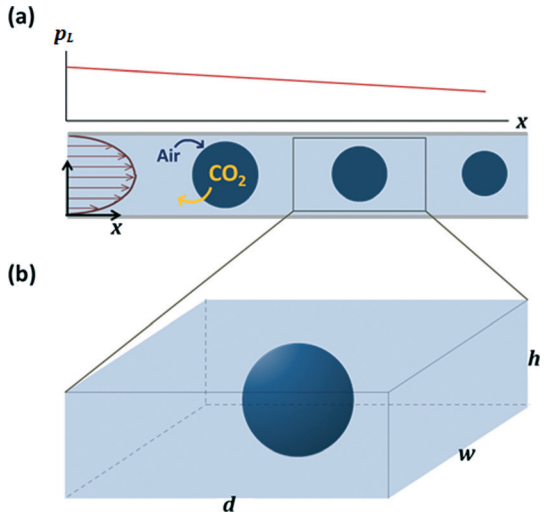

Fig. 3 Schematic of the model CO_2 dissolution problem. (a) The bubbles are assumed to move approximately with the same speed as the liquid phase, and so the problem is simplified to (b) an isolated gas bubble dissolving in a static liquid. *d*, *w*, and *h* are the distance between two bubbles, width and height of the channel, respectively. The liquid pressure (p_L) around the bubbles linearly decreases along the channel. In the stationary bubble dissolution model, p_L is a linear function of time and position, as sketched in (a).

in the liquid can be approximated as zero. According to our calculations, the liquid in the channel is never saturated during the entire experiment.

On the other hand, it is possible, from the observation of the rapid dissolution of CO_2 bubbles in the first 30 ms (Fig. 2(a–c)), that there is 'local' saturation of CO_2 near the interface. However, accumulated CO_2 must diffuse away from the interface on the time scale of $t_D \sim a_0^2/D \cong 100$ ms, where the diffusion coefficient for CO_2 in water is $D \cong 2.1 \times 10^{-9}$ m^2 s^{-1}. Furthermore, this calculation cannot explain the constant size of the bubbles in a long channel (Fig. 2(c)). Therefore, the local situation cannot explain the appearance of the apparent equilibrium regime.

We now consider one other mechanism to explain the constant bubble radius. We hypothesize that other dissolved gases in the liquid phase (unless the liquid is strictly degassed immediately before the experiment), can diffuse into the CO_2 bubbles while CO_2 is diffusing out from the bubble. As a result, the bubble radius reaches an equilibrium value. Considering the effect of other gases on the dissolution is reasonable in our system because the amount of dissolved air in an aqueous solution with dimensions $d \times w \times h$ is comparable to the amount of CO_2 in the initial bubble. It is thus likely that highly soluble CO_2 diffuses rapidly out of the bubble in the early stage so the bubble radius is reduced and, after 30 ms, in-flow of other gases maintains the gas pressure in equilibrium with the liquid pressure so that the bubble obtains a constant size. Based on this concept, we next develop a theoretical model for the dissolution of a CO_2 bubble in a microfluidic channel. Since we varied the concentrations of SDS solution in the experiments, the effect of surface tension γ is included in the analysis. A linear decrease in liquid pressure (p_L) along the channel is also considered in the model. Finally, we will show how the initial composition of the bubble affects the dissolution, and propose an explanation for the effects of SDS on the first regime of the dissolution.

Theory

We describe a theoretical model to characterize gas exchange between the bubble and the liquid surroundings. Our model of the dissolution is shown in Fig. 3, which shows the side view of the channel. Once a bubble is generated in the channel, CO_2 in the bubble starts to diffuse into the liquid and air (*e.g.* N_2 and O_2) that is dissolved in the liquid phase starts to diffuse into the bubble. We assume that the flow is fully developed from the beginning of the main channel. Along the channel, there is linear drop of pressure in the liquid flow, of which the gradient varies linearly with the liquid flow rate. As described in Fig. 3, dissolution of the bubbles flowing with the liquid can be analysed by studying single bubble dissolution in a liquid box of dimensions $d \times w \times h$. The model follows the basic outline of Weinberg and Subramanian[18] and we include the influence of surface tension and the change of the external pressure in time.

We demonstrate in the ESI† that a CO_2 bubble does not saturate the liquid phase nor the periphery of the bubble, hence for the short times characteristic of the microfluidic experiments, the problem can be simplified to a stationary gas bubble dissolving in an infinite liquid phase. The liquid pressure p_L, which is linearly decreasing along the channel, can be regarded as a linearly decreasing function in time if we follow one bubble and monitor the liquid pressure in the neighbourhood of the bubble. Among many gases that possibly exist in the liquid, we only include O_2 and N_2 as the gases other than CO_2 in the system and simply refer to O_2 + N_2 as air. The dissolution problem is then modelled with several more assumptions about the system: the bubble is a perfect sphere at any time, gases diffuse into and out of the bubble in only the radial direction, and the gases obey the ideal gas law. Even though the gas bubbles are much smaller than the channel geometry, there can be convective effects that can accelerate the dissolution of gas bubbles. The Peclet number (Pe) characterizing our system can be estimated by $\mathrm{Pe} = \dot{\gamma}a^2/D$, where $\dot{\gamma}$, a and D are, respectively, the typical shear rate in the channel, the typical bubble radius, and the diffusion coefficient of CO_2. The shear rate $\dot{\gamma}$ is approximately $\dot{\gamma} \sim \langle v \rangle/h \sim 10^{-2}$ ms^{-1}/10^{-5} m = 10^3 s^{-1}, where $\langle v \rangle$ is the mean flow velocity and h is the channel height. The corresponding scale of the Peclet number is $\mathrm{Pe} = \dot{\gamma}a^2/D \sim [10^3\ \mathrm{s}^{-1} \times (10^{-6}\ \mathrm{m})^2]/(10^{-9}\ \mathrm{m}^2\ \mathrm{s}^{-1}) = 10^0$, which suggests the importance of diffusion. Therefore, we expect convection effects in the channel to be modest, and for simplicity we model the dissolution as a diffusion dominated process.

On the liquid side, gases obey the radial diffusion equation,

$$\frac{\partial c_i}{\partial t} = \frac{D_i}{r^2}\frac{\partial}{\partial r}\left(r^2\frac{\partial c_i}{\partial r}\right), \tag{1}$$

where c_i and D_i are the mass concentration and the diffusivity of the i^{th} gas component, and i = 1, 2, 3 denote, respectively, CO_2, O_2, and N_2. The boundary conditions are,

$$c_i(t, a(t)) = c_{is} \tag{2a}$$

$$c_i(t, \infty) = c_{i\infty} \tag{2b}$$

$$c_i(0, r) = c_{i\infty}(r > a_0), \tag{2c}$$

where $a(t)$ is the bubble radius, which changes with time, c_{is} is the mass concentration of the i^{th} gas at the interface on the liquid side, $c_{i\infty}$ is the initial concentration of the i^{th} gas far from the bubble, and $a_0 = a(0)$ is the initial bubble radius.

Mass conservation in the bubble, requires

$$\frac{\mathrm{d}}{\mathrm{d}t}\left(\frac{4}{3}\pi a^3\rho_i\right) = 4\pi a^2 D_i\left(\frac{\partial c_i}{\partial r}\right)_a, \tag{3}$$

where ρ_i is the mass density of i^{th} gas in the bubble, and the change of mass density of each gas is matched with the flux at the interface. By rearranging terms and applying the ideal gas law, we get

$$\frac{1}{R_{gi}T}\left(p_i\frac{\mathrm{d}a}{\mathrm{d}t} + \frac{a}{3}\frac{\mathrm{d}p_i}{\mathrm{d}t}\right) = D_i\left(\frac{\partial c_i}{\partial r}\right)_a, \tag{4}$$

where R_{gi}, T, p_i are, respectively, the specific gas constant of the i^{th} gas, temperature, and partial pressure of i^{th} gas. Letting $\alpha_1 = R_{g2}/R_{g1}$ and $\alpha_2 = R_{g3}/R_{g1}$ and summing up the three equations for different components of (4), we find

$$\begin{aligned}\frac{1}{R_{g1}T}\left[(p_1+p_2+p_3)\frac{\mathrm{d}a}{\mathrm{d}t} + \frac{a}{3}\left(\frac{\mathrm{d}p_1}{\mathrm{d}t}+\frac{\mathrm{d}p_2}{\mathrm{d}t}+\frac{\mathrm{d}p_3}{\mathrm{d}t}\right)\right] \\ = D_1\left(\frac{\partial c_1}{\partial r}\right)_a + \alpha_1 D_2\left(\frac{\partial c_2}{\partial r}\right)_a + \alpha_2 D_3\left(\frac{\partial c_3}{\partial r}\right)_a\end{aligned} \tag{5}$$

In the bubble dissolution system, we have the liquid pressure $p_L(t)$ that always balances the gas pressure, therefore,

$$p_1 + p_2 + p_3 = p_L + \frac{2\gamma}{a}, \tag{6}$$

where γ is the interfacial tension. The time-rate-of-change of the partial pressures of gas are obtained by differentiating eqn (6):

$$\frac{\mathrm{d}p_1}{\mathrm{d}t} + \frac{\mathrm{d}p_2}{\mathrm{d}t} + \frac{\mathrm{d}p_3}{\mathrm{d}t} = \frac{\mathrm{d}p_L}{\mathrm{d}t} - \frac{2\gamma}{a^2}\frac{\mathrm{d}a}{\mathrm{d}t} \tag{7}$$

By substituting eqn (6) and (7) into (5), an equation for the radius change is obtained,

$$\frac{\mathrm{d}a}{\mathrm{d}t} = \frac{D_1\left(\frac{\partial c_1}{\partial r}\right)_a + \alpha_1 D_2\left(\frac{\partial c_2}{\partial r}\right)_a + \alpha_2 D_3\left(\frac{\partial c_3}{\partial r}\right)_a - \frac{a}{3R_{g1}T}\left(\frac{\mathrm{d}p_L}{\mathrm{d}t}\right)}{\frac{1}{R_{g1}T}\left(p_L + \frac{4\gamma}{3a}\right)}. \tag{8}$$

The concentration gradients at the interface for any of the three gas components can be obtained by solving eqn (1) with the given boundary conditions[31]

$$\left(\frac{\partial c_i}{\partial r}\right)_a = (c_{i\infty} - c_{is})\left(\frac{1}{a} + \frac{1}{\sqrt{\pi D_i t}}\right) \tag{9}$$

Mass concentrations at the interface (c_{is}) and in the far field ($c_{i\infty}$) can be rewritten in terms of pressure by applying Henry's law,

$$c_{is} = k_i p_i, \tag{10}$$

and

$$c_{1\infty} = 0 \text{ (initial } CO_2 \text{ concentration in liquid phase)} \tag{11a}$$

$$c_{2\infty} = k_2 p_{O_2} \text{ (p_{O_2}: partial pressure of } O_2 \text{ in the atmosphere)} \tag{11b}$$

$$c_{3\infty} = k_3 p_{N_2} \text{ (p_{N_2}: partial pressure of } N_2 \text{ in the atmosphere).} \tag{11c}$$

Here, p_{O_2} and p_{N_2}, are the partial pressure of O_2 and N_2 in the atmosphere and are not to be confused with p_2 and p_3, which are the partial pressures in the bubble. Since the SDS solution used in our experiments was placed under atmospheric pressure, the concentrations of O_2 and N_2 in the bulk liquid are proportional to their partial pressures. By substituting the mass fluxes in eqn (8) to (9), and applying Henry's law and eqn (6), eqn (8) becomes

$$\begin{aligned}\frac{\mathrm{d}a}{\mathrm{d}t} = \frac{R_{g1}T}{\left(p_L + \frac{4\gamma}{3a}\right)}\Bigg\{&-D_1k_1p_1\left(\frac{1}{a} + \frac{1}{\sqrt{\pi D_1 t}}\right) + \alpha_1 k_2 D_2 \\ &\times\left(p_{O_2} + p_1 + p_3 - \left(p_L + \frac{2\gamma}{a}\right)\right)\left(\frac{1}{a} + \frac{1}{\sqrt{\pi D_2 t}}\right) \\ &+ \alpha_2 k_3 D_3\left(p_{N_2} - p_3\right)\left(\frac{1}{a} + \frac{1}{\sqrt{\pi D_3 t}}\right) \\ &- \frac{a}{3R_{g1}T}\left(\frac{\mathrm{d}p_L}{\mathrm{d}t}\right)\Bigg\}\end{aligned} \tag{12}$$

Eqn (12) provides an evolution equation for $a(t)$ and clearly shows that the radius change of a bubble is determined by the change of the partial pressures of gases in the

bubble, the liquid pressure, and the interfacial tension. Together with the equations for p_1, p_3 and p_L, the dissolution system can be solved. For example, from eqn (4)

$$\frac{dp_1}{dt} = -\frac{3p_1}{a}\left[D_1 k_1 R_{g1} T\left(\frac{1}{a} + \frac{1}{\sqrt{\pi D_1 t}}\right) + \frac{da}{dt}\right], \quad (13)$$

and

$$\frac{dp_3}{dt} = \frac{3}{a}\left[\alpha_2 D_3 k_3 R_{g1} T\left(p_{N_2} - p_3\right)\left(\frac{1}{a} + \frac{1}{\sqrt{\pi D_3 t}}\right) - p_3\frac{da}{dt}\right]. \quad (14)$$

Finally, p_L can be obtained directly from Darcy's law, which describes viscous pressure-driven flow in a narrow channel (ESI†) and can be written as

$$p_L = \frac{\beta\mu Q^2}{w^2 h^4}\left(t - \frac{Lwh}{Q}\right) + p_{atm}, \quad (15)$$

where μ and Q are respectively, the shear viscosity and the volumetric flow rate of the liquid phase, p_{atm} is the pressure at the end of the channel, and w, h, and L are, respectively, the width, height, and total length of the channel. Also, β is a constant that depends on the cross-sectional shape of the channel.

Now we have all the equations – eqn (12)–(15) – that describe the gas bubble dissolution system. By solving these equations numerically, $a(t)$, $p_1(t)$, and $p_3(t)$ can be obtained, and with eqn (6), $p_2(t)$ can also be obtained. To effectively visualize the behaviour of bubble radius and partial pressures as a function of time, and to reduce the number of variables, eqn (12)–(15) are nondimensionalized. The nondimensional parameters are defined as:

$$\bar{r} = r/a_0 \quad (16a)$$

$$R(\tau) = a(t)/a_0 \quad (16b)$$

$$Q_1 = D_2/D_1 \quad (16c)$$

$$Q_2 = D_3/D_1 \quad (16d)$$

$$\tau = tD_1/a_0^2 \quad (16e)$$

$$\Gamma = \gamma/(a_0 P_{atm}) \quad (16f)$$

$$B_1 = k_2/k_1 \quad (16g)$$

$$B_2 = k_2/k_3 \quad (16h)$$

$$A = k_1 R_{g1} T \quad (16i)$$

$$\Phi = 1/(B_1 A) \quad (16j)$$

$$\bar{p}_1 = p_1/p_{atm},\ \bar{p}_2 = p_2/p_{atm},\ \bar{p}_3 = p_3/p_{atm},\ \bar{p}_L = p_L/p_{atm}. \quad (16k)$$

Therefore, the nondimensionalized equations are

$$\begin{aligned}\frac{dR}{d\tau} = -\frac{1}{5\Phi\left(\bar{p}_L + \frac{4\Gamma}{3R}\right)}\Bigg\{&5\bar{p}_1\left[\frac{1}{B_1}\left(\frac{1}{R} + \frac{1}{\sqrt{\pi\tau}}\right) - \alpha_1 Q_1\left(\frac{1}{R} + \frac{1}{\sqrt{\pi Q_1\tau}}\right)\right] \\ &+ 5\bar{p}_3\left[\frac{\alpha_2 Q_2}{B_2}\left(\frac{1}{R} + \frac{1}{\sqrt{\pi Q_2\tau}}\right) - \alpha_1 Q_1\left(\frac{1}{R} + \frac{1}{\sqrt{\pi Q_1\tau}}\right)\right] \\ &- \alpha_1 Q_1\left(1 - 5\left(\bar{p}_L + \frac{2\Gamma}{R}\right)\right)\left(\frac{1}{R} + \frac{1}{\sqrt{\pi Q_1\tau}}\right) \\ &- \frac{4\alpha_2 Q_2}{B_2}\left(\frac{1}{R} + \frac{1}{\sqrt{\pi Q_2\tau}}\right) + \frac{5\Phi R}{3}\left(\frac{d\bar{p}_L}{d\tau}\right)\Bigg\},\end{aligned} \quad (17)$$

$$\frac{d\bar{p}_1}{d\tau} = -\frac{3\bar{p}_1}{R}\left[A\left(\frac{1}{R} + \frac{1}{\sqrt{\pi\tau}}\right) + \frac{dR}{d\tau}\right], \quad (18)$$

$$\frac{d\bar{p}_3}{d\tau} = \frac{3\bar{p}_3}{R}\left[\frac{\alpha_2 Q_2 B_1 A}{B_2}\left(\frac{4}{5\bar{p}_3} - 1\right)\left(\frac{1}{R} + \frac{1}{\sqrt{\pi Q_2\tau}}\right) - \frac{dR}{d\tau}\right], \quad (19)$$

and

$$\bar{p}_L = \frac{\beta\mu Q^2}{w^2 h^4 p_{atm}}\left(\frac{\tau a_0^2}{D_1} - \frac{Lwh}{Q}\right) + 1. \quad (20)$$

For typical liquid flow rate (Q = 25 μL min^{-1}) and pure water viscosity μ,[29] eqn (20) can be simplified to

$$\bar{p}_L = 1 - 0.05(\tau - 4), \quad (21)$$

and $\bar{p}_L$ in the eqn (17) can be replaced by eqn (21). Then there are three equations and three unknowns (R, $\bar{p}_1$, $\bar{p}_3$). These equations can be solved numerically, and as mentioned in previous section, we focus on the effects of Γ, $\bar{p}_L$, and $\bar{p}_1$ (0) (initial amount of CO_2 in the bubble) in analysing the behaviour of $R(\tau) = a/a_0$

Discussion

Effect of gas exchange on the dissolution of CO_2 bubbles

Eqn (17)–(20) are solved numerically and plotted (Fig. 4). No adjustable parameters are used to fit the experimental data. In order to compare directly the calculations with experimental results, all the graphs are plotted as nondimensional radius (or partial pressure) change *versus* dimensional time.

In Fig. 4(a), the radius change of a bubble obtained from both the experiment and the model are plotted. The model calculations show two regimes, rapid shrinking and equilibrium, and are in good agreement with the experiment at 8 mM SDS solution. For the same parameter values, Fig. 4(b) shows the model calculations of the partial pressure change of CO_2 and air in the bubble. All CO_2 diffuses out from the bubble in the first 60 ms and simultaneously the air enters the bubble. After 60 ms, the bubbles contain only air, and the pressure of air in the bubble linearly decreases with time because it remains in equilibrium with the liquid pressure in the channel. In this regime, the sizes of the bubbles remain very nearly constant.

The results of Fig. 4(a, b) demonstrate the effect of external gases on the equilibrium regime of CO_2 bubble dissolution. In order to further explore this idea, we developed control experiments using degassed liquid, which provide more direct evidence to the effect of other gases in the liquid phase (Fig. 4(c)). We degassed the continuous phase as explained in the experimental section. Comparing to the original experiments, in the degassed solution CO_2 bubbles reached smaller equilibrium radii, but did not completely disappear, which would be expected if the continuous phase was completely free of dissolved gases. Since our experimental method does not allow the liquid to be degassed completely under atmospheric conditions (the SDS solution is degassed under vacuum but brought back to the atmospheric pressure for the experiments), we believe that there is a small amount of air in the degassed solution. In particular, our model calculations with reduced (1% of the atmospheric condition) external gas in the liquid phase show good agreement with the degassed experiment results at 8 mM SDS. Also, the equilibrium radius is smaller by a factor of 3 compared to the non-degassed case.

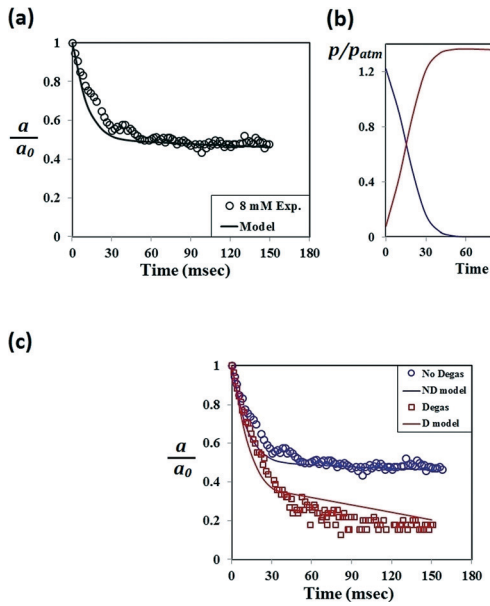

Fig. 4 (a) Change of the nondimensional radius *versus* dimensional time as calculated from the multicomponent dissolution model and compared with the experiment results in a 8 mM SDS solution. Also, the calculation was done for the initial bubble of 95% CO_2, where $\bar{p}_1(0)$ = 1.22 (as described in the text). (b) Change of nondimensionalized partial pressures of CO_2 and air in the bubble plotted *versus* dimensional time. After 60 ms, the nondimensionalized air partial pressure ($\bar{p}_2 + \bar{p}_3$) is in equilibrium with the liquid pressure $\bar{p}_L$, which decreases linearly with time. The gas exchange in the bubble leads to an apparent equilibrium behaviour of CO_2 gas bubbles in the microfluidic channel. (c) Nondimensionalized radius plotted *versus* time for the experiments done with 8 mM SDS and degassed 8 mM SDS solutions. Solid lines are obtained from the multicomponent model. For the model calculation of the degassed case, we assumed that the amount of air dissolved in the SDS solution was 1% of the normal case.

To examine possible effects of different parameters, we further test the multicomponent mathematical model at different (nondimensionalized) interfacial tensions (γ) and liquid pressures (p_L) (Fig. 5(a, b)). Since the liquid pressure was controlled by the flow rate (Q) of the liquid phase, results provided in Fig. 5(b) are the bubble radii at different liquid flow rates. Both Fig. 5(a, b) show that the CO_2 bubble dissolution $R(\tau) = a/a_0$ is not affected by the change of interfacial tension and the range of liquid flow rates we used in the experiment. However, in the experiment, the concentration of SDS was varied from a value much lower than the CMC to 2.5 CMC, which is expected to affect both interfacial tensions and the dissolution behaviours.

The calculated radii shown in Fig. 5(a) demonstrate that it is not the interfacial tension that controls the dissolution behaviour. Therefore our results suggest that when we add SDS in water, the SDS molecules not only lower the interfacial tension, but also play the role of a diffusion barrier so that the CO_2 bubble dissolution rate varies with the concentration of SDS. Detailed arguments on the barrier idea are discussed in the following section.

Effect of SDS on the initial bubble composition

Considering the unique environment of the flow-focusing channel where the bubble is generated by "cutting" of the gas flow by the liquid flowing through two branches of the inlet channel, we conclude that the exchange of components between the gas and liquid phases starts from the point

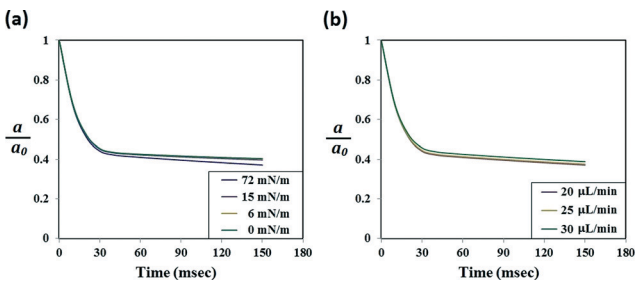

Fig. 5 Test of the multicomponent dissolution model for different parameters. (a) Radius changes calculated in the model at different surface tension values (γ = 72, 15, 6, 0 mN m^{-1}). (b) Radius changes calculated for different liquid flow rates – different p_L – (at Q = 20, 25, 30 μL min^{-1}).

where the two phases meet each other. In that sense, since there must be gas exchange during the pinch-off process, the first bubble generated in the main channel is not necessarily a pure CO_2 bubble as some in-flow of other dissolved gases could have occurred. The role of surfactant (SDS) in this stage is to sit on the gas–liquid interface to form a layer that lowers the diffusion rates of gases (Fig. 6(a)).[32] We expect that as the gas bubbles are generated they are covered by SDS molecules and that the coverage is higher at higher concentrations. Thus, when the concentration of SDS is high enough ($C_{SDS} \geq$ CMC (= 8 mM)), SDS molecules cover the entire gas–liquid interface and block the diffusion of air into the bubble, which results in a gas bubble containing nearly 100% CO_2. Consequently, these bubbles dissolve rapidly throughout the channel to reach relatively small equilibrium radii compared to experiments at low concentrations of SDS (*e.g.* Fig. 2(a, b)).

Based on the idea that the concentration of SDS molecules can affect the initial composition of the gas bubble in the channel, the effect of this initial composition on the final radius of bubbles is plotted in Fig. 6(b). The equilibrium radius is calculated from the model based on different values of initial CO_2 partial pressure $\bar{p}_1$ (0). According to the calculations, the higher the partial pressure of CO_2 in the initial bubble, the smaller equilibrium radius it reaches.

Model calculations at different initial partial pressures are plotted with the experiment data in Fig. 6(c). The curves obtained for $\bar{p}_1$ (0) = 0.2, 0.67, 1.04 and 1.22 fit the experiment data for C_{SDS} = 0.5, 1, 4, and 8 mM, respectively. Initial pressures are chosen from the range between $\bar{p}_1$ (0) = 0 (no CO_2 in the bubble) and $\bar{p}_1$ (0) = 1.29 (pure CO_2 bubble). The calculations show good agreement with the experimental results at different SDS concentrations, and thus, it can be concluded that different dissolution behaviour of bubbles in the rapid dissolution regime is controlled by the initial composition of bubbles. Detailed investigation on the effects of the surfactant layer on the bubble formation at the flow-focusing junction, as well as the resulting composition of the initial bubble, remain as future topics for research.

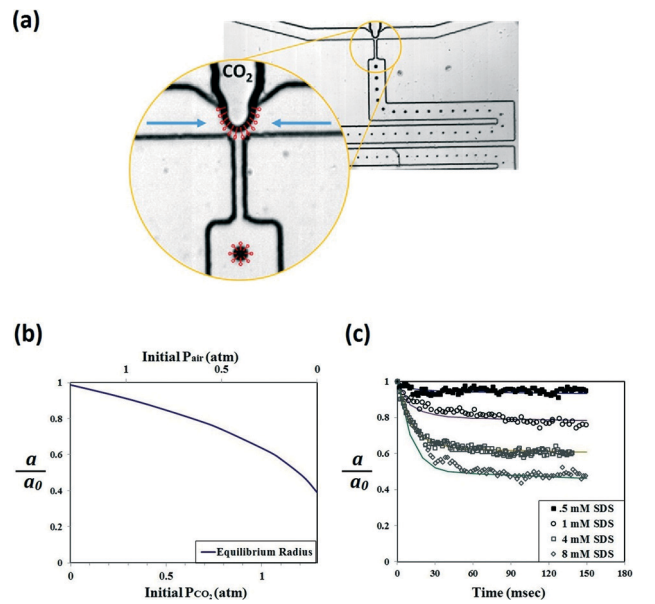

Fig. 6 (a) A model of SDS layer blocking other gases (air) in the liquid phase from diffusion into the bubble at the flow-focusing inlet. The arrows indicate the liquid flow. (b) Nondimensionalized equilibrium radius predicted from the model plotted *versus* initial partial pressure of CO_2 in the bubble. Assuming that the interfacial tension is the air–water value, the initial partial pressure of CO_2 in pure CO_2 bubble is 1.29 atm. (c) Radius change obtained from the multicomponent model at different initial pressures are fitted to the experimental results obtained at different surfactant concentrations. From the top curve to the bottom (solid lines are the model results), radius changes are calculated at $\bar{p}_1$ (0) = 0.2, 0.67, 1.04 and 1.22, respectively. There is good agreement between the model and the experimental results, which demonstrates our idea that the amount of surfactant in the liquid phase affects the gas exchange rate at the bubble generation stage so that the bubbles start dissolving with different initial compositions.

Conclusions

Microfluidic experiments on CO_2 dissolution were performed and theoretical analysis was made by considering multicomponent gas exchange. In the experiments using a flow-focusing microfluidic channel, CO_2 bubbles dissolved for 30 ms and reached an equilibrium size. Bubbles showed different behaviours at different concentrations of SDS in the liquid phase: for concentrations lower than CMC, bubbles shrank more rapidly to reach a smaller final size as the concentration got closer to the CMC, and for the concentrations higher than CMC, bubbles showed the same behaviour regardless of the surfactant concentration. The two-regime feature of the CO_2 bubble dissolution was explained by diffusion of other gases (air) that were already dissolved in the liquid phase.

In the theoretical model, a single gas bubble in an infinite liquid phase was considered, and we assumed that there are three gases escaping from and entering the bubble. Since the experiments were performed during pressure-driven flow in a microfluidic channel using surfactant solutions, linearly decreasing liquid pressure and the effect of interfacial tension was also included in the model. The model showed a good agreement with experimental results obtained at high concentrations of SDS ($C_{SDS} \geq$ CMC (= 8 mM)), and together with the experiments performed in degassed SDS solution, the two distinct regimes were well explained. Different dissolution behaviours at concentrations lower than CMC were explained by introducing a diffusion barrier idea at the bubble generation stage. Our hypothesis was that the initial bubble in the experiment may have different compositions based on the concentration of surfactant molecules in the liquid phase. Considering different initial compositions of the bubbles in the multicomponent model, the dissolution behaviours at SDS concentrations lower than CMC were rationalized. Detailed investigation of gas diffusion at the bubble generation stage needs to be done, but it is reasonable and important to consider in-flux

of other gases into a gas bubble in such experiments using microfluidic channels and small-sized bubbles.

Acknowledgements

We acknowledge support from the Samsung Scholarship, Samsung Foundation of Culture (to S. Shim). J. Wan and P. Panchal thank support from the Kate Gleason College of Engineering at RIT, the Faculty Education and Development Grant and Texas Instruments/Douglass Harvey Faculty Development Award. J. Wan acknowledges the Donors of the American Chemical Society Petroleum Research Fund for partial support of this research. H. A. Stone acknowledges support from the Princeton Environmental Institute.

References

1 D. M. D'Alessandro, B. Smit and J. R. Long, *Angew. Chem., Int. Ed.*, 2010, **49**, 6058–6082.
2 S. K. Al Mansoori, E. Itsekiri, S. Iglauer, C. H. Pentland, B. Bijeljic and M. J. Blunt, *Int. J. Greenh. Gas Control*, 2010, **4**, 283–288.
3 K. Z. House, D. P. Schrag, C. F. Harvey and K. S. Lackner, *Proc. Natl. Acad. Sci. U. S. A.*, 2006, **103**, 12291–12295.
4 N. J. House, D. D. Faulder, G. L. Olson and J. R. Fanchi, *Society of Petroleum Engineers*, 2003.
5 P. Argyropoulos, K. Scott and W. M. Taama, *Electrochim. Acta*, 1999, **44**, 3575–3584.
6 G. Q. Lu and C. Y. Wang, *J. Power Sources*, 2004, **134**, 33–40.
7 C. Litterst, S. Eccarius, C. Hebling, R. Zengerle and P. Koltay, *J. Micromech. Microeng.*, 2006, **16**, S248–S253.
8 Q. Xu, M. Nakajima, Z. Liu and T. Shiina, *Int. J. Mol. Sci.*, 2011, **12**, 462–475.
9 T.-L. Neoh, H. Yoshii and T. Furuta, *J. Inclusion Phenom. Macrocyclic Chem.*, 2006, **56**, 125–133.
10 E. Stride and M. Edirisinghe, *Soft Matter*, 2008, **4**, 2350.
11 P. H. Calderbank and A. C. Lochiel, *Chem. Eng. Sci.*, 1964, **19**, 485–503.
12 K. Tsuchiya, H. Mikasa and T. Saito, *Chem. Eng. Sci.*, 1997, **52**, 4119–4126.
13 P. G. Brewer, E. T. Peltzer, G. Friederich and G. Rehder, *Environ. Sci. Technol.*, 2002, **36**, 5441–5446.
14 Y. Liao and J. B. McLaughlin, *Chem. Eng. Sci.*, 2000, **55**, 5831–5850.
15 P. S. Epstein and M. S. Plesset, *J. Chem. Phys.*, 1950, **18**, 1505.
16 P. B. Duncan and D. Needham, *Langmuir*, 2004, **20**, 12.
17 R. B. Bird, W. E. Stewart and E. N. Lightfoot, *Transport Phenomena*, JohnWiley & Sons, New York, 2002.
18 M. C. Weinberg and R. S. Subramanian, *J. Am. Ceram. Soc.*, 1980, **63**, 527–531.
19 M. C. Weinberg, *Chem. Eng. Sci.*, 1981, **36**, 137–141.
20 M. Abolhasani, M. Singh, E. Kumacheva and A. Gunther, *Lab Chip*, 2012, **12**, 1611–1618.
21 T. Cubaud, M. Sauzade and R. Sun, *Biomicrofluidics*, 2012, **6**, 22002–220029.
22 S.-A. Leung, J. B. Edel, R. C. R. Wootton and A. J. deMello, *Meas. Sci. Technol.*, 2004, **15**, 290–296.
23 R. Sun and T. Cubaud, *Lab Chip*, 2011, **11**, 2924–2928.
24 K. Fei, W. H. Chen and C. W. Hong, *Microfluid. Nanofluid.*, 2007, **5**, 119–129.
25 J. I. Park, Z. Nie, A. Kumachev, A. I. Abdelrahman, B. P. Binks, H. A. Stone and E. Kumacheva, *Angew. Chem., Int. Ed.*, 2009, **48**, 5300–5304.
26 J. I. Park, Z. Nie, A. Kumachev and E. Kumacheva, *Soft Matter*, 2010, **6**, 630.
27 S. G. Lefortier, P. J. Hamersma, A. Bardow and M. T. Kreutzer, *Lab Chip*, 2012, **12**, 3387–3391.
28 E. Tumarkin, Z. Nie, J. I. Park, M. Abolhasani, J. Greener, B. Sherwood-Lollar, A. Gunther and E. Kumacheva, *Lab Chip*, 2011, **11**, 3545–3550.
29 A. Q. Shen, B. Gleason, G. H. McKinley and H. A. Stone, *Phys. Fluids*, 2002, **14**, 4055.
30 S. R. P. D. Rocha and K. P. Johnston, *Langmuir*, 2000, **16**, 3690–3695.
31 H. S. Carslaw, *Introduction to the Mathematical Theory of the Conduction of Heat in Solids*, Dover Publications, New York, 1945.
32 G. Hebrard, J. Zeng and K. Loubiere, *Chem. Eng. J.*, 2009, **148**, 132–138.

